The Astrophysical Journal, 577:961–973, 2002 October 1

CHEMICAL EVOLUTION OF THE CIRCUMSTELLAR ENVELOPES OF CARBON-RICH POST–ASYMPTOTIC GIANT BRANCH OBJECTS

F. Herpin,[1] J. R. Goicoechea, J. R. Pardo,[2] and J. Cernicharo[2]
Instituto de Estructura de la Materia, Departamento de Física Molecular, CSIC, Serrano 121, E-28006 Madrid, Spain
Received 2002 February 19; accepted 2002 June 9

ABSTRACT

We have observed, with the 30 m IRAM telescope, the Caltech Submillimeter Observatory telescope, and the *Infrared Space Observatory* (*ISO*) satellite,[3] the rotational lines of CO at millimeter, submillimeter, and far-IR wavelengths in the direction of carbon-rich stellar objects at different stages of evolution: CRL 2688 (a very young proto–planetary nebula), CRL 618 (a proto–planetary nebula), and NGC 7027 (a young planetary nebula). Several changes in the longwave emission of CO and other molecules are discussed here in relation with the degree of evolution of the objects. In the early stages, represented by CRL 2688, the longwave emission is dominated by CO lines. In the intermediate stage, e.g., CRL 618, very fast outflows are present which, together with the strong UV field from the central star, dissociate CO. The released atomic oxygen is seen via its atomic lines and allows the formation of new O-bearing species, such as H_2O and OH. The abundance of HNC is enhanced with respect to HCN as a result of the chemical processes occurring in the photodissociation region. At this stage, CO lines and [O I] lines are the dominant coolants, while the cooling effect of [C II] is rising. At the planetary nebula stage, e.g., NGC 7027, large parts of the *old* CO AGB material have been reprocessed. The spectrum is then dominated by atomic and ionic lines. New species, such as CH^+, appear. Water has probably been reprocessed in OH.

Subject headings: infrared: stars — line: identification — planetary nebulae: individual (CRL 618, CRL 2688, NGC 7027) — stars: abundances — stars: carbon — stars: evolution

1. INTRODUCTION

Solar-type stars remain in the asymptotic giant branch (AGB) for about 10^6–10^7 yr, losing mass through stellar winds ($\dot{M} \sim 10^{-4}$ to 10^{-7} $M_\odot$ yr^{-1} and ejection velocity $\sim$5–25 km s^{-1}; see, e.g., Loup et al. 1993). During this phase, the ejected material progressively forms an expanding circumstellar envelope (CSE). Molecular species are easily formed in the innermost regions of the CSE. Some of these molecules aggregate onto dust grains, which under the action of radiation pressure accelerate and push the remaining gas, producing an expanding dusty molecular envelope. UV photons from the interstellar radiation field dissociate gas-phase molecules in the external layers of the envelopes, allowing new chemical reactions and the production of new molecular species. These chemical changes have been very well studied through observations and models in the case of IRC +10216, the prototypical carbon-rich AGB star (Glassgold 1996; Cernicharo, Guélin, & Kahane 2000 and references therein). Additional changes in the composition of the CSE do occur when the central object starts its evolution toward the white dwarf stage. A large UV field arises from the central (much hotter) star, and at the same time high-velocity winds (HVWs) appear and interact with the AGB remnant (Cernicharo et al. 1989; Kwok 2000). Objects in this phase are called proto–planetary nebulae (PPNs). During this period (1000–2000 yr; Bujarrabal et al. 2001), the almost spherical symmetry typical of the AGB stage disappears and is replaced by a complicated geometrical structure (most PPNs are elliptical, bipolar, or quadrupolar; Zuckerman & Aller 1986; Frank et al. 1993). The chemical composition is also strongly affected by these processes: O-bearing molecules can be formed in carbon-rich objects (Herpin & Cernicharo 2000), and complex organic molecules, which are not observed in IRC +10216, are efficiently produced (Cernicharo et al. 2001a, 2001b).

In order to better understand this evolution, we present in this paper a comparative study of the millimeter, submillimeter, and far-IR CO line emission from three objects representing different stages of this fast transition: CRL 2688, a very young PPN; CRL 618, a PPN; and NGC 7027, a young planetary nebula (PN). The different excitation conditions of the observed CO lines allow us to probe different layers in the CSEs. In particular, we study the CSE remnant wind and the higher velocity winds. The CSE component is the "normal" AGB wind, and the wind component refers to a higher velocity wind, which is probably not present during the AGB phase and which contributes to changing the morphology from spherical to bipolar or other nonspherical geometries. The observations are presented in § 2. The representativity of each selected source is discussed in § 3. Section 4 is devoted to the analysis of the spectra of IRC +10216 as a representative of the AGB phase. In § 5 we discuss the wind structure of the young PPN CRL 2688. Section 6 is devoted to CRL 618 and § 7 to the analysis of NGC 7027 observations. An overall comparative discussion of the four objects is then presented in § 8.

[1] Current address: Observatoire de Bordeaux, B.P. 89, F-33270 Floirac, France; herpin@observ.u-bordeaux.fr.
[2] Also visiting scientist at Division of Physics, Mathematics, and Astronomy, California Institute of Technology, MS 320-47, Pasadena, CA 91125.
[3] Based on observations with *ISO*, an ESA project with instruments funded by ESA member states (especially the PI countries: France, Germany, the Netherlands, and the United Kingdom) and with participation of ISAS and NASA.

2. OBSERVATIONS AND DATA ANALYSIS

The IRAM 30 m observations of the CO $J = 1$–0 and 2–1 lines were performed in 2000 September using four SIS receivers with high (greater than 0.90) image sideband rejection. The pointing and focus were checked against either Saturn or Jupiter, using the continuum emission of the sources, and was found to be accurate to within 2″. The typical system temperatures during these observations were 250 K (CO $J = 1$–0) and 400 K (CO $J = 2$–1). The observations used the wobbler system, which provides very flat baselines. The spectrometers were a filter bank (at 115 GHz) and an autocorrelator (at 230 GHz) set to cover a band of 512 MHz with frequency resolutions of 1 and 1.25 MHz, respectively (velocity resolutions of 2.60 and 1.63 km s^{-1}, respectively).

The CO $J = 3$–2, 4–3, 6–5, and 7–6 observations were performed with the 10.4 m telescope of the Caltech Submillimeter Observatory (CSO) at the summit of Mauna Kea (Hawaii) in 2000 September and October with three different receivers based on helium-cooled SIS mixers operating in double-sideband mode (DSB). The typical system temperatures during these observations were 750 K (CO $J = 3$–2) and 5000–6000 K (CO $J = 4$–3, 6–5, and 7–6). For further details about the receivers, see Kooi et al. (2000) and references therein. The back ends were two different acousto-optical spectrometers (AOSs). One of them covers a bandwidth of 500 MHz with 1024 channels, and the other one covers 1.5 GHz with 2048 channels, thus providing, respectively, the following velocity resolutions (in km s^{-1}): $146.38/\nu$ and $219.57/\nu$, with ν in GHz. The instantaneous band of the receivers, however, is $\sim$0.9 GHz, thus limiting the validity of the data from the 1.5 GHz AOS to that range.

Since some of the CSO observations were performed shortly after a new 790–920 GHz receiver was installed for the first time at the telescope, its pointing and focus were carefully determined during runs earlier in the year. Then, the pointing of this and the other receivers was checked during our observations, using Jupiter and Saturn first and then the CO emission of each object. Taking into account that this emission is somewhat extended, the pointing is considered accurate to within 4″ (CO $J = 3$–2 and 4–3 lines) and 2″ (CO $J = 6$–5 and 7–6 lines). The observations were also performed by wobbling the secondary reflector by 60″. Proper corrections were finally applied to the data to compensate for the use of only one load (ambient temperature) in the chopper-wheel standard calibration of the CSO that relies upon the Penzias & Burrus (1973) approximation.

For the comparative discussion that we make in this paper, fits of the CO millimeter/submillimeter observations (shown in Fig. 1) of the three objects have been performed to derive the flow velocity of the different components and the integrated intensity ratio R_I between the emission of the CSE remnant and that of the wind for each transition. As angular resolution changes when observing at different frequencies and with different telescopes, the relative contribution to the bulk of the detected emission from the CSE remnant (extended) and the HVWs (unresolved) will be different. Hence, R_I outlines the wind excitation of the different flows across the envelope (see Tables 1, 4, and 6).

The *ISO* long-wavelength spectrometer (LWS) Fabry-Pérot (FP) data ($\lambda/\Delta\lambda \sim 9500$) of CRL 2688 were obtained during orbits 366 and 369. The integration times are 3400 and 5800 s. The spectral resolution is 0.015 μm. The LWS grating mode (43–196.7 μm, $\lambda/\Delta\lambda \sim 200$) has a spectral resolution of 0.29 μm for the 43–93 μm range and 0.6 μm for the 80–196 μm range. LWS01 grating spectra for CRL 2688 and CRL 618 were taken during orbits 21 and 688, respectively (total on-source times of 1218 and 5360 s, respectively). The $J = 18$–17 line of HCN was observed toward CRL 2688 during orbit 154 with the LWS grating mode and an integration time of 914 s (see Fig. 2). Finally, the LWS grating spectra of NGC 7027 taken by *ISO* during orbits 21, 342, 349, 356, 363, 377, 537, 552, 559, 566, 579, 587, 594, 601, 706, 713, 720, 727, 734, 741, 755, 762, 769, 776, and 783 were averaged. The total on-source time was 53409 s. All data were processed following pipeline number 9 and treated with ISAP[4] to remove glitches and fringes.

3. REPRESENTATIVITY OF THE SOURCE SAMPLE

In the next sections we try to identify and discuss the changes that occur through the transition of a carbon-rich AGB star to the PN stage. The aim of this work is to trace the evolution of the circumstellar chemistry in the late-AGB and post-AGB phases. This study is based on the analysis of the spectral differences observed in four objects: IRC +10216, CRL 2688 (the Egg Nebula), CRL 618, and NGC 7027. We thus have to rely on the assumption that IRC +10216 will evolve into an object similar to the Egg Nebula and then to an object similar to CRL 618, which will finally evolve to a PN that looks like NGC 7027. The ideal, but unfeasible approach, would be to observe a single object evolving through the post-AGB phase. In addition, our sample objects should be "typical" in the sense that each one should represents the average characteristics of the bulk of objects in the same stage of evolution.

However, CRL 2688, CRL 618, and NGC 7027 seem to be quite unusual objects in some properties, extreme cases among all carbon-rich AGB and post-AGB objects. All are very bright in molecular lines, but while IRC +10216 is a relatively close source (110–150 pc; Groenewegen, van der Veen, & Matthews 1998; Crosas & Menten 1997), the other three objects are 5–10 times farther away (Acker et al. 1992; Bujarrabal, Fuente, & Omont 1994; Sahai et al. 1998). This may twist the comparison between IRC +10216 and the other sources, as distance influences line fluxes and profiles.

Recent works estimate a $\leq 2\ M_\odot$ progenitor mass for IRC +10216 and place its core mass at 0.6 $M_\odot$ (Kahane et al. 2000). Theoretical calculations suggest a progenitor main-sequence mass of $\sim 3\ M_\odot$ for both CRL 2688 and CRL 618 (Speck, Meixner, & Knapp 2000) and 3–4 $M_\odot$ for NGC 7027 (Bernard Salas et al. 2001). IRC +10216 therefore, seems likely to evolve to the PN phase rather more slowly than the others, and this may affect the chemistry of the envelope. Anyway, several parallels exist between these objects: dense, optically thick, dusty CSEs and shell-like density enhancements observed as incomplete arcs (Men'shchikov et al. 2001; Mauron & Huggins 1999). These circumstellar concentric arcs, extremely pronounced in IRC +10216, are also detected in NGC 7027 (see Kwok, Su, & Stoesz 2001). More generally, it has been proposed that further evolution of CRL 2688 will lead to morphologies similar to those observed in NGC 7027 (especially the ionized nebula and H_2 region; Cox et al. 1997).

[4] The *ISO* Spectral Analysis Package (ISAP) is a joint development by the LWS and SWS Instrument Teams and Data Centers. Contributing institutes are CESR, IAS, IPAC, MPE, RAL, and SRON.

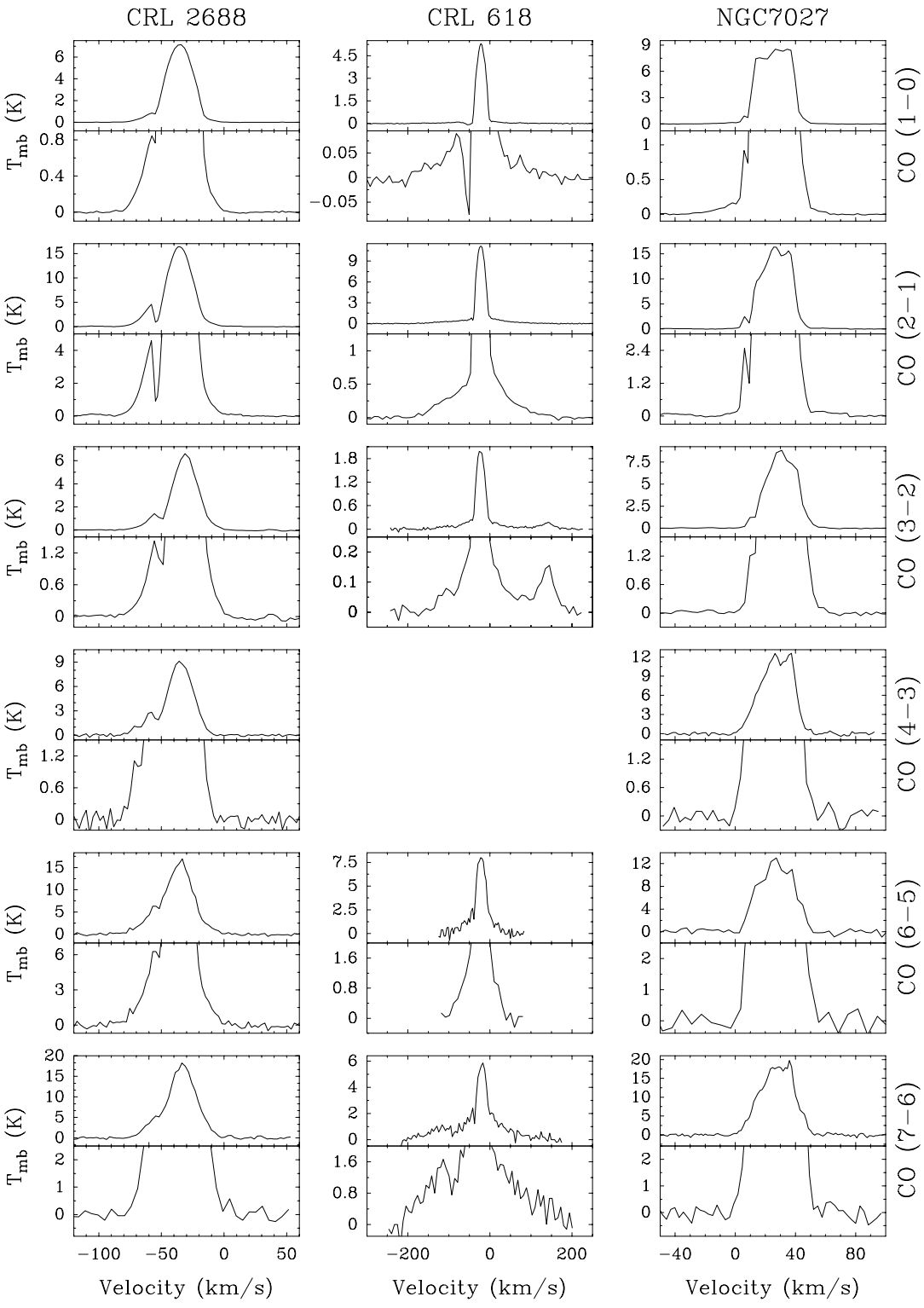

FIG. 1.—Spectra for the ^{12}CO $J = 1$–0, 2–1, 3–2, 4–3, 6–5, and 7–6 transitions for CRL 2688, CRL 618 (no $J = 4$–3 observation), and NGC 7027. The main beam temperatures are in kelvins and the velocity is in kilometers per second. Baselines were applied. The $J = 1$–0 and 2–1 lines are IRAM 30 m observations; the others were made with the CSO. Lines are smoothed. For each line, the upper panel shows the whole profile and the lower panel shows the high-velocity emission with an expanded vertical scale. Note that the emission present on the red part (at 141 km s^{-1}) of the CO ($J = 3$–2) emission from CRL 618 is the HC_3N ($J = 38$–37) line emission (at 345.609 GHz). The conversion factors in janskys per kelvin are, respectively, 4.3, 4.2, and 40 for the $J = 1$–0 and 2–1 observations and all other observations.

The Egg Nebula is quite anomalous, compared with more usual carbon-rich post-AGB objects. Its infrared spectrum is very different from that of any other carbon-rich post-AGB object, since it appears to be optically thick even at 30 μm (Omont et al. 1995). More common are the most extreme dusty carbon stars, such as the small group of sources discussed by Volk, Xiong, & Kwok (2000).

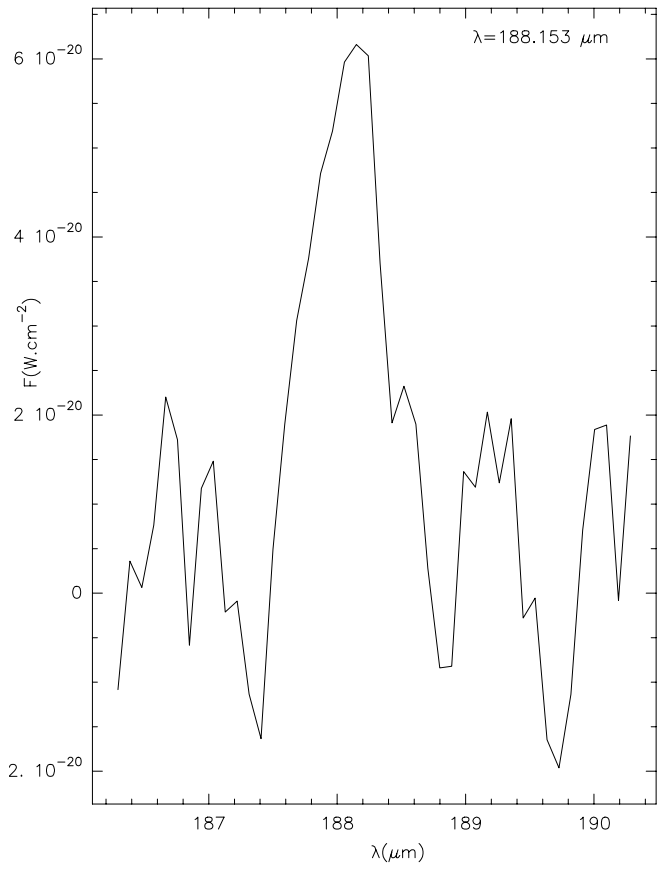

FIG. 2.—HCN $J = 18$–17 line emission detected by the LWS grating in CRL 2688 at a resolution of 0.6 μm (S/N $\sim$ 4).

CRL 618 is quite similar to CRL 2688 in that both have massive molecular envelopes and central bipolar outflows (Meixner et al. 2001). However, CRL 618 shows an unusually rich circumstellar chemistry that could be related to its advanced stage of evolution (Herpin & Cernicharo 2000).

NGC 7027 is quite unusual among PNs in that it has a relatively massive CSE beyond the ionized region. Its photodissociation region (PDR) is one of the densest and warmest in the PN sample studied by Liu et al. (2001). In fact, the ionized region is known to be relatively low in mass ($\leq$0.2 $M_\odot$, smaller than the typical values of 0.3–0.5 $M_\odot$ of the ionized region of PN) while the surrounding, mostly molecular gas totals 2–4 $M_\odot$.

In conclusion, the objects selected here are rather peculiar in some properties that may influence their post-AGB evolution. However, a comparative study of their molecular envelopes could be useful in identifying the distinct chemistries induced by the general physical changes produced by the different degrees of evolution, and this is the aim of this paper.

4. IRC +10216: THE PROTOTYPICAL CARBON-RICH AGB OBJECT

To introduce this study, it is useful to present the main features of a typical object at the end of the AGB stage. IRC +10216 is the brightest carbon-rich AGB star. Its estimated distance is 110–150 pc (Groenewegen 1997; Crosas & Menten 1997). It is believed to be in the final stage of red giant evolution and exhibits a bipolar reflection nebula (Skinner, Meixner, & Bobrowsky 1998). The temperature of the central object is 2000 K, and the expansion velocity of the CSE is 14.5 km s^{-1} (Skinner et al. 1998; Cernicharo et al. 2000). IRC +10216 has an extended CSE in which more than 50 molecular species have been detected (see line surveys by Cernicharo et al. 1996, 2000). This object has a rich carbon chemistry, and many of the species detected in its molecular envelope are carbon chain radicals, which are formed in the external layers of the CSE (Cernicharo et al. 1996, 2000). The innermost regions of the envelope are dominated by a chemistry at thermodynamical equilibrium (Tsuji 1973), in which CO, HCN, C_2H_2, SiO are formed. As shown by Cernicharo et al. (1996), the far-IR spectrum consists of strong dust emission and several molecular emission lines from ^{12}CO ($J = 14$–13 to $J = 39$–38), ^{13}CO (^{12}CO/^{13}CO $\sim$ 45), HCN ($J = 18$–17 to $J = 48$–47), H^{13}CN, and vibrationally excited HCN. The HCN lines have intensities similar to those of CO, and HCN/CO = 1/10, proving that HCN is the main coolant in the innermost region of the CSE. Only one ion, HCO^+, has been detected (Lucas & Guélin 1999), and there is no [C II] line emission. The mid- and near-IR spectra are dominated by the rovibrational lines of C_2H_2 and HCN (Cernicharo et al. 1999). The most abundant molecules through the CSE are CO, HCN, and C_2H_2 (Fuente, Cernicharo, & Omont 1998; Cernicharo et al. 2000).

The molecular observations of this object are well explained by a photochemical model (Glassgold 1996) considering that, because of the low effective temperature of the central star, the only UV photons available in the outer CSE come from the interstellar radiation field.

5. A YOUNG PPN: CRL 2688

CRL 2688 is a very young PPN (it left the AGB phase probably only about 100 yr ago) with an effective temperature around 6600 K (spectral type F5; Justtanont et al. 1997) and luminosity close to 1.8×10^4 $L_\odot$ (Jura & Kroto 1990). The nondetection of [O I] and [C II] (Cox et al. 1996) indicates that radiation from the central star has not yet formed a PDR. The molecular gas is in expanding, fragmented shell structures, and shocks are thought to heat it (Cox et al. 1996). The AGB CSE expansion velocity is 20 km s^{-1}. CO emission has been seen as far as 42″ from the central object. The weaker ^{13}CO emission extends over 20″ (Yamamura et al. 1996). Sahai et al. (1998) detected a moderate-velocity wind (hereafter MVW) of 40 km s^{-1}, with an angular extension of 10″. High-velocity gas emerging in two different directions from the central star has been detected by Cox et al. (2000) in the CO $J = 2$–1 emission line. The size of the emitting region is 4″, with extensions in both the north-south and east-west directions. Cox et al. (2000) have shown that this high-velocity gas is closely related to the H_2 emission at 2 μm.

5.1. *Low-Excitation* CO *lines*

The profiles of all low-excitation CO lines (see Fig. 1) are characteristic of optically thick emission. However, while the $J = 1$–0, 2–1, and 3–2 lines probably trace the extended AGB remnant envelope of CRL 2688, higher J transitions are more sensitive to hotter gas from the inner layers of the envelope and hence of lower spatial extent. As J increases,

TABLE 1
PARAMETERS FOR THE DIFFERENT FLOWS IN CRL 2688

CO LINE ($J=$)	v_{main} (km s^{-1})	v_{wing} (km s^{-1})	R_I	ΔR_I
1–0	19.3	50.0	0.08	(0.01)
2–1	20.0	52.0	0.08	(0.01)
3–2	23.9	50.7	0.11	(0.01)
4–3	24.1	40.3	0.16	(0.02)
6–5	23.4	41.6	0.24	(0.02)
7–6	23.3	33.3	0.24	(0.03)

NOTES.— The uncertainty on v_{main} and v_{wing} is 0.3 km s^{-1}. R_I is the wing and main integrated intensities ratio.

the line opacities in the AGB CSE decrease and the emerging profiles change accordingly.

From the CO observations of CRL 2688 and the line parameters given in Table 1, we can distinguish two main outflows. The main one, the AGB CSE remnant, is centered at -35.4 km s^{-1} and covers around 20 km s^{-1} (in good agreement with Young et al. 1992). The second outflow has a moderate velocity extent, $\simeq$50 km s^{-1}, and is centered at -60 km s^{-1}. The intensity of the red wing of this MVW is weaker than that of its blue counterpart in the CO lines. We believe that this behavior is produced by AGB CSE remnant absorption of the MVW red wing.

An absorption dip is detected in the blue part of the millimeter and submillimeter CO lines at $\simeq -55$ km s^{-1}, just at the terminal velocity of the AGB CSE. It suggests that the low-velocity wind absorbs radiation from the inner and faster wind. Young et al. (1992) found that this absorption has a velocity width of $\simeq$1 km s^{-1} in the low-J lines. We found the same value for the CO $J = 6$–5 and 7–6 lines. This would suggest that the microturbulence through the AGB CSE is nearly constant and equal to 1 km s^{-1}.

The ratio R_I goes from 0.08 ($J = 1$–0) to 0.24 ($J = 7$–6), stressing the importance of the MVW emission in the intermediate-J CO lines. The dilution of the MVW-emitting region in the telescope beam will change with J. In addition, line opacities for the AGB CSE remnant and the MVW will also change differently with J. Hence, above a given rotational transition, the emission from the AGB CSE remnant will be weaker than that from the MVW. Observations of high-excitation lines are thus needed in order to follow up the CO emission from the inner envelope.

5.2. *Far-IR Emission*

Far-IR observations reveal the inner and hotter regions of the CSE, where important chemical and physical processes are changing the structure of the AGB CSE. Rotational lines of ^{12}CO ($J = 14$–13 to $J = 26$–25) are clearly detected, while the emission from ^{13}CO is very weak. HCN is clearly detected in the AOT LWS02 grating spectrum of its $J = 18$–17 transition (see Fig. 2, line detected with signal-to-noise ratio [S/N] of $\sim$4; all the subpeaks are smoothed noise). Note that some CO lines present broad wings at the grating resolution (see $J = 19$–18, 20–19, and 21–20) that are probably instrumental artifacts resulting from the defringing of the LWS data.

Several high-J CO (from $J = 16$–15 to $J = 26$–25) lines were observed in FP mode with the LWS (see Fig. 3 for the $J = 16$–15, 19–18, 24–23, and 26–25 lines). The fluxes were divided by the continuum and rescaled to the values obtained for the same lines with the LWS grating. To derive more valuable information about kinematics, and because the excitation and opacity are rather similar in all these lines, we computed an average spectrum (better S/N) of all the individual lines (i.e. Fig. 3, *right panel*). Study of this average CO LWS/FP spectrum reveals a line much broader than what we could expect from the AGB CSE remnant and centered at -65 km s^{-1}. It could suggest that all the emission is coming from the MVW. In order to estimate the CO emission at high J from the AGB CSE remnant and from the MVW, we have fitted two Gaussians to the average spectrum of Figure 3. We obtain velocities of -70 ± 10 and -35 ± 10 km s^{-1} (see in the same figure the modeled emission from our large velocity gradient [LVG] calculations, discussed below). These velocities agree, within the FP absolute wavelength calibration, with the MVW and AGB CSE velocities, respectively. Obviously, higher spectral resolution observations are required to confirm both components (i.e., Herschel Telescope observations with HIFI). In the following, we assume that both components emit in the high-J lines of CO, and we try to derive the relative contribution of each one.

Obviously, the average spectrum does not directly provide information on the column density of CO. In order to derive this parameter we have fitted the CO $J = 16$–15 emission observed with the FP (the line with the best S/N) with the two velocity components derived from the average spectrum. We then extended the result to the other lines (Fig. 3, *left panel*). Globally, the lines are well fitted by our model, with column densities of 85% (feature at -70 km s^{-1}) and 45% (feature at -35 km s^{-1}) with respect to the values retrieved from fitting the grating spectrum.

The red counterpart of the emission at -70 km s^{-1} is not detected. Our lines suggest that one part of the emission (at -70 km s^{-1}) comes from a wind with an outflow velocity of about 35 km s^{-1}, probably the MVW of Sahai et al. (1998). As the -70 km s^{-1} emission comes from a region where large shocks occur (interaction with the AGB remnant envelope), and the column density is thought to be larger, this emission appears stronger.

The other component (at the stellar velocity) is consistent with the wind velocity derived from our CO mm and submm observations (see Table 1). The widths of the emissions in each CO line show that the velocity dispersion is probably important in the excitation region.

In order to model the observed emission, we have used an LVG code, which divides the emitting source into several components with different solid angles (defined by θ). For each component we have fitted the column density of the molecule under consideration, the H_2 volume density, and the temperature. Hence, the molecular abundance will depend on the layer thickness, which cannot be derived in this retrieval scheme. While these assumptions could be correct for the high-velocity wings and the PDR (CRL 618 and NGC 7027), the component corresponding to the AGB remnant is poorly approximated, as the whole CSE is reduced to a layer with a given average column density, temperature, and density. This AGB remnant has been modeled in detail by Bujarrabal & Alcolea (1991).

The same basic physical parameters have been applied to ^{13}CO and HCN, and we then only varied the column densities (see parameters in Table 2). For all the objects, model components were selected according to previous observational and theoretical works and our millimeter and submilli-

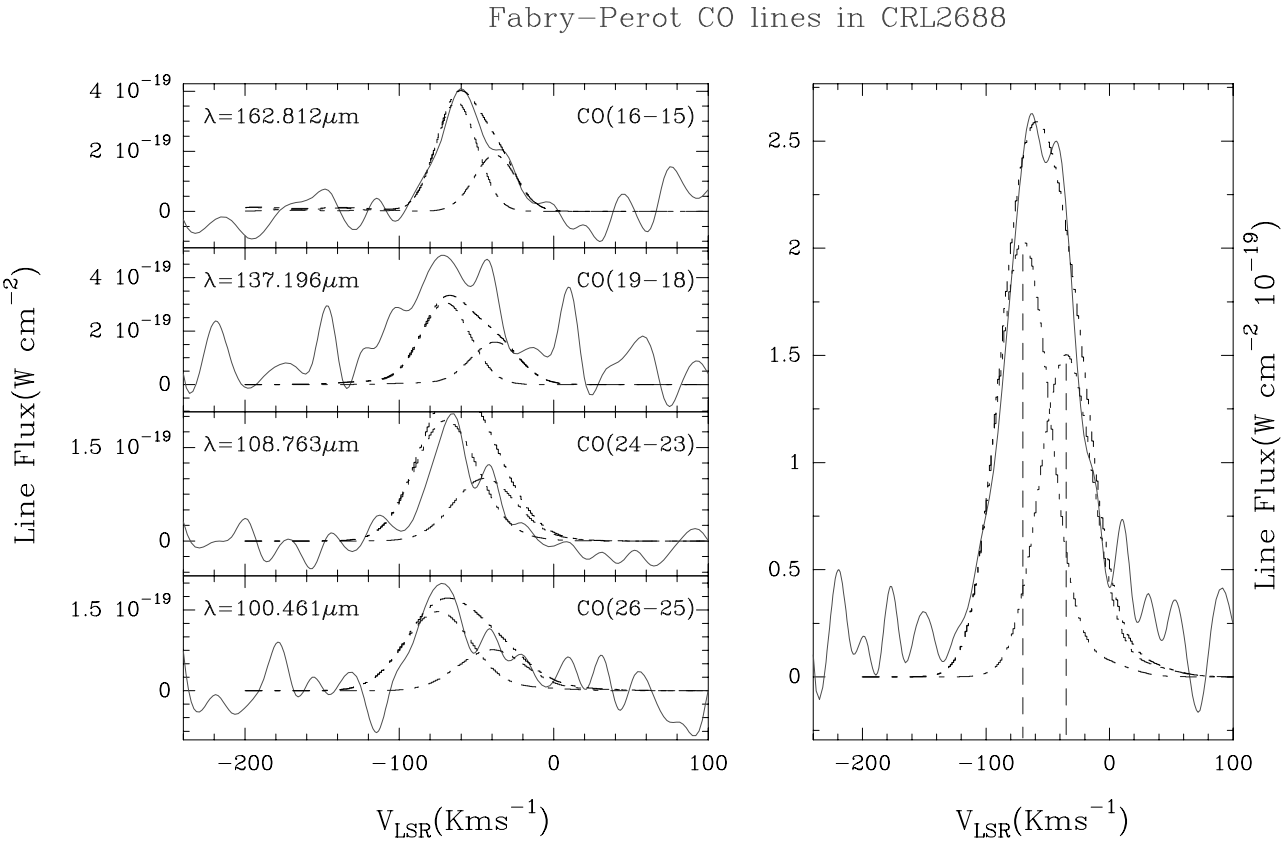

FIG. 3.—LWS/FP observations of ^{12}CO lines in CRL 2688 (*left*) and average spectra of all observed CO lines (*right*). The intensity scale corresponds to the continuum normalized flux rescaled to the values obtained with the LWS gratings for the same lines. The wavelength of each transition is indicated at the top left corner of each panel. Dashed lines show the fit produced by our LVG model as described in the text (with a center velocity precision of ± 15 km s^{-1}).

meter observations. The particular temperatures, solid angles, velocity, and density are also derived from these studies, even if in some cases we adapt the parameters to correctly fit the data. Of course, column densities for each layer are sensitive to the excitation temperature.

According to other authors and our study of the low-*J* CO line emission, the adopted geometry model and physical parameters of each component are

1. An inner region representing the fast wind from the star (Sahai et al. 1998) and modeled as a layer with $\theta = 0\farcs3$, expansion velocity of 100–200 km s^{-1}, temperature of 800 K, and density of 5×10^7 cm^{-3}. The ^{12}CO column density (N) is 2×10^{18} cm^{-2} and the ^{13}CO and HCN abundances relative to ^{12}CO are less than 1/25 and less than 1/100, respectively. This hot component is needed to fit correctly the high-*J* CO lines, as the single 400 K component of Cox et al. (1996) does not seem to be sufficient, in our view.

2. As this fast wind slows down when colliding with the outer parts of the envelope, we have considered intermediate layers of larger sizes. Parameters are from Cox et al. (1996, 2000): a layer with temperature of 500 K, $\theta = 2''$, expansion velocity of 100 km s^{-1}, and density of 5×10^7 cm^{-3}. The ^{12}CO column density has decreased to 7×10^{17} cm^{-2}, and the HCN/^{12}CO abundance ratio is less than 1/30. An additional component is required when the wind has slowed down to 60 km s^{-1}, with a temperature of 400 K, $\theta = 3''$, density of 5×10^7 cm^{-3}, and $N(^{12}\mathrm{CO}) = 5 \times 10^{17}$ cm^{-2}. ^{13}CO and HCN have the same relative abundance ratios as in the previous layer.

TABLE 2

COLUMN DENSITIES OBTAINED FROM OUR MODEL FOR ALL MOLECULES PRESENT IN EACH REGION OF CRL 2688

	CONDITIONS				COLUMN DENSITY		
REGION	T (K)	θ[a] (arcsec)	v (km s^{-1})	$n(\mathrm{H_2})$ (cm^{-3})	^{12}CO (cm^{-2})	^{13}CO (cm^{-2})	HCN (cm^{-2})
Fast wind from the star	800	0.3	200	5×10^7	2×10^{18}	$<8 \times 10^{16}$	$<2 \times 10^{16}$
	500	2	100	5×10^7	7×10^{17}	$<2.8 \times 10^{16}$	$<2.3 \times 10^{16}$
	400	3	60	5×10^7	5×10^{17}	$<2 \times 10^{16}$	$<1.7 \times 10^{16}$
Medium wind from the star.....	250	15	40	5×10^7	4.5×10^{16}	$<1.8 \times 10^{15}$	$<1.5 \times 10^{15}$
AGB remnant	50	25	20	5×10^5	3.5×10^{16}	$<1.4 \times 10^{15}$	$<1.2 \times 10^{15}$

[a] The solid angle of each considered layer.

TABLE 3
OBSERVED AND PREDICTED INTENSITIES FOR THE MILLIMETER AND SUBMILLIMETER CO LINES FOR EACH SOURCE

	CRL 2688		CRL 618		NGC 7027	
CO LINE ($J=$)	I_{obs} (Jy)	I_{mod} (Jy)	I_{obs} (Jy)	I_{mod} (Jy)	I_{obs} (Jy)	I_{mod} (Jy)
1–0	30	10	23	21	36	24
2–1	70	30	47	66	70	83
3–2	271	296	79	197	364	475
4–3	373	429	...	400	516	498
6–5	640	650	320	742	520	893
7–6	760	790	232	994	840	1061

3. An MVW region (Sahai et al. 1998) with $\theta = 15''$, temperature of 250 K, density of 5×10^7 cm^{-3}, velocity of 40 km s^{-1}, and ^{12}CO column density of 4.5×10^{16} cm^{-2}. The relative abundances for the other species are the same as for previous layers.

4. The AGB remnant CSE, where low-excitation CO emission extends beyond 40″ (Cox et al. 1996; Yamamura et al. 1996), which we have modeled as a layer with $\theta = 25''$ at 50 K, expansion velocity of 20 km s^{-1}, and $N(^{12}\mathrm{CO}) = 3.5 \times 10^{16}$ cm^{-2}.

The global fit is shown in Figure 4 and reproduces reasonably well the LWS *ISO* grating observations of CRL 2688. We also applied the same model to the millimeter and submillimeter CO lines. Components 3 and 4 mainly fit the low-J CO lines (millimeter and submillimeter lines). Observed and predicted intensities are in good agreement (see Table 3).

5.3. *Changes Since the Previous Stage*

With respect to the previous AGB stage, represented by IRC +10216, we see that the molecules emitting in the far-IR are basically the same, but with different relative intensities. This is probably due to the fact that the innermost region of the AGB remnant envelope has already been pushed away in these initial stages of the evolution toward the PPN phase. Hence, all the rovibrational lines of HCN have disappeared, not necessarily because of a depletion of this molecule, but because of the lack of sufficiently high temperatures and densities. This fact, together with the lack of [O I] and [C II], makes CO the main coolant of the envelope. The observational evidence of winds faster than those in the previous stage indicates that the gas in the inner layers is now heated by shocks, where the high-J CO line excitation is favored. The presence of polyynes, as shown by the *ISO* mid-IR spectrum of this object (Cernicharo et al. 2001b), indicates that the envelope has also started an important chemical evolution when compared with IRC +10216. The HVWs and the increasing UV field from the central object are at the origin of this new chemistry, and this will be enhanced in the next stage (CRL 618).

6. A PPN OBJECT: CRL 618

CRL 618 is one of the few clear examples of an AGB star in the transition phase to the PN stage. There is evidence that this object must be a ~200 yr old PPN (Bujarrabal et al. 1988). It has a compact H II region created by a hot central star (30,000 K, spectral type B0; Justtanont et al. 1997). CRL 618 is seen as a bipolar nebula at optical, radio, and infrared wavelengths (Carsenty & Solf 1982; Bujarrabal et al. 1988; Cernicharo et al. 1989; Neri et al. 1992; Hora et al. 1996). The expansion velocity of the outer envelope is around 20 km s^{-1}. CO observations by Cernicharo et al. (1989) showed evidence of the presence of a high-velocity outflow (~200 km s^{-1}). The UV photons from the central star and this HVW perturb the CSE, producing shocks and PDRs, which modify the physical and chemical conditions of the gas (Herpin & Cernicharo 2000; Cernicharo et al. 2001a, 2001b).

The molecular content of CRL 618 (J. Cernicharo et al. 2002, in preparation) is characterized by a large abundance of cyanopolyynes, acetylenic chains, methane, methylpolyynes, and benzene (Cernicharo et al. 2001a, 2001b): this PPN is a very efficient organic chemistry factory. The detection of long carbon chains in both CRL 618 and CRL 2688 suggests that the input of a UV radiation field from the evolving central object and/or the action of HVWs on the slowly expanding AGB remnant modify the CSE chemistry, allowing the formation of new and more complex molecules.

6.1. *Low-Excitation* CO *lines*

Two outflows can be seen in the CO line profiles of CRL 618 (see Table 4). The main outflow is centered at −22.0 km s^{-1}, with an expansion velocity of roughly 20 km s^{-1}. The optically thick CO $J = 1$–0 line clearly absorbs the continuum from −60 to −40 km s^{-1}, coinciding with the main outflow terminal velocity. Other lines (higher transitions) show an absorption dip (self-absorption). In CRL 618, many molecular lines show P Cygni profiles at 3 and 2 mm (J. Cernicharo et al. 2002, in preparation). These lines, which correspond to very high energy rovibrational levels of HC_3N and HC_5N, are formed in the PDR of the high-density torus surrounding the central object.

The HVW (around 200 km s^{-1}), associated with a biconical outflow, is also observed in many other molecular transitions (see also Cernicharo et al. 1989; J. Cernicharo et al. 2002, in preparation), but with a smaller velocity span. The CO wings corresponding to this outflow have a smooth triangular shape and are present in all the millimeter and submillimeter lines. Their intensity increases with J, R_I going from 0.09 for $J = 1$–0 to an estimated value of more than 2.6 in the $J = 7$–6 line. Therefore, the emission in the high-J lines (§ 6.2) is basically dominated by this HVW component.

TABLE 4
PARAMETERS FOR THE DIFFERENT FLOWS IN CRL 618

CO LINE ($J=$)	v_{main} (km s^{-1})	v_{wing} (km s^{-1})	R_I	ΔR_I
1–0	19.7	202.5	0.09	(0.01)
2–1	19.6	204.5	0.22	(0.02)
3–2	18.9	178.5	0.45	(0.03)
6–5	17.1	>76.0	>0.72	(0.05)
7–6	18.8	≥195.0	≥2.6	(0.3)

NOTES.—The uncertainty on v_{main} and v_{wing} is 0.3 km s^{-1}. R_I is the wing and main integrated intensities ratio. For the 6–5 and 7–6 lines, the parameters v_{wing} and R_I are lower limits, because of the unsufficient bandwidth available for these observations.

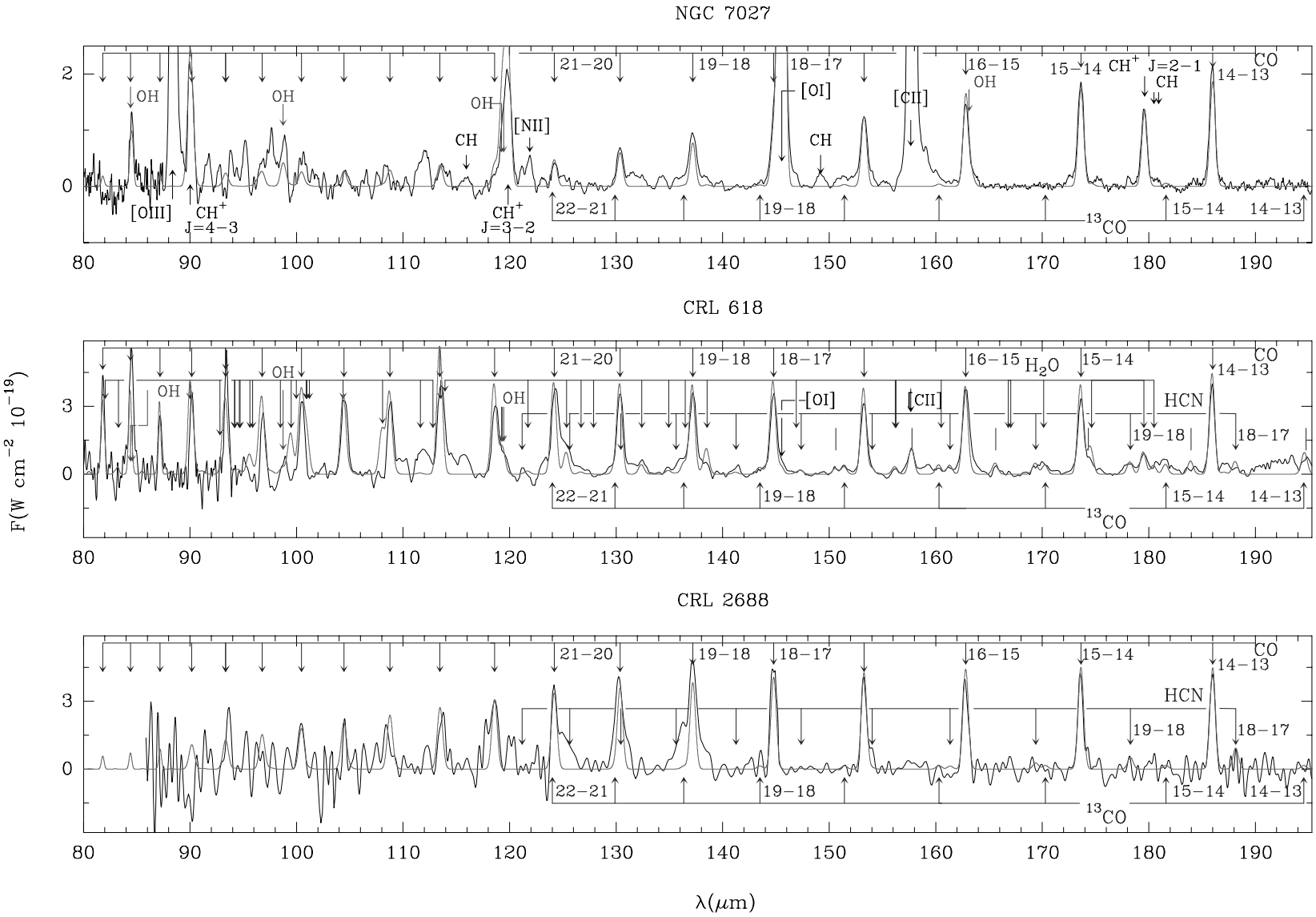

FIG. 4.—Continuum-subtracted LWS spectra of CRL 2688 (*bottom*), CRL 618 (*middle*), and NGC 7027 (*top*). The result of our models is shown by the solid gray line. The lines of ^{12}CO, ^{13}CO, HCN, H_2O, CH^+, and OH are indicated by arrows, while those of HNC in CRL 618 are indicated by vertical lines (from $J = 22$–21 at 150.627 μm to $J = 17$–16 at 194.759 μm). The [C II] and [O III] lines are not included in our models; the plots indicate Gaussian fits to these features.

TABLE 5

COLUMN DENSITIES OBTAINED FROM OUR MODEL FOR ALL MOLECULES PRESENT IN EACH REGION OF CRL 618

	CONDITIONS				COLUMN DENSITY						
REGION	T (K)	θ[a] (arcsec)	v (km s^{-1})	$n(H_2)$ (cm^{-3})	^{12}CO (cm^{-2})	^{13}CO (cm^{-2})	HCN (cm^{-2})	HNC (cm^{-2})	o-H_2O (cm^{-2})	OH (cm^{-2})	[O I] (cm^{-2})
Torus (including PDR)	250	1.5	20	5×10^7	10^{19}	5×10^{17}	10^{16}	10^{16}	3×10^{17}	8×10^{15}	...
	800	1.1	20	5×10^7	6×10^{17}	3×10^{16}	...	...	...	...	...
	1000	0.6	20	7×10^7	10^{19}	5×10^{17}	...	...	...	...	4.5×10^{19}
HVW	200	1.7	50	10^7	5×10^{18}	2.5×10^{17}	3×10^{17}	2×10^{17}	...	...	...
	1000	1.5	200	10^7	2×10^{16}	1×10^{15}	2×10^{15}	10^{14}	...	...	...
AGB remnant	50	10	20	10^5	7×10^{17}	3.5×10^{16}	7×10^{16}	7×10^{14}	...	...	...

[a] The solid angle of each considered layer.

6.2. *Far-IR Emission*

The rotational lines of ^{12}CO ($J = 14$–13 to $J = 41$–40), ^{13}CO ($J = 14$–13 to $J = 19$–18), HCN, HNC, [O I] (at 63.170 and 145.526 μm), and [C II] ($^2p_{3/2}$–$p_{1/2}$ transition at 157.74 μm) are observed in CRL 618 (see Fig. 4). Several lines of OH and H_2O are also detected. However, no H_2O emission has been detected at 183 GHz. As the 22, 183, and 321 GHz water maser lines are collisionally excited (radiative effects are small) in warm dense gas (Neufeld & Melnick 1990, 1991), this nondetection may indicate that water is not in the wind region, but rather in the torus.

The model used for analyzing the LWS observations of CRL 618 was presented in Herpin & Cernicharo (2000). Briefly, it consists of a central, high-density torus, with its inner part being a PDR, an extended AGB remnant envelope, and high-velocity bipolar outflows. The physical parameters of the different layers are given in Table 5. The AGB remnant parameters are derived from Yamamura et al. (1994) and Hajian, Phillips, & Terzian (1996). The HVW characteristics are from Cernicharo et al. (1989), Neri et al. (1992), and Martín-Pintado et al. (1995). Justtanont et al. (2000) fit the *ISO* CO lines with a 700 K component [$n(H_2) = 5 \times 10^7$ cm^{-3}]. Temperatures of the torus layers have been varied in order to get the best fit of the data. Our model, once applied to the low-excitation CO lines, disagrees with the observed $J = 3$–2 to $J = 7$–6 intensities. This may be mainly explained by the completely nonspherical geometry of the source and by the complex velocity field across the envelope. Moreover, as the CO molecules are reprocessed, excitation is more complex and cannot be reproduced by our relatively simple model.

6.3. *Changes Since the Previous Stage*

As in the previous, very young PPN phase, shock chemistry plays an important role, as even faster outflows are detected. The now higher effective temperature of the central star induces a UV-based chemistry dominated by the photolysis of key molecules, and the molecular content has started to be reprocessed. This fact is proved by the observed changes in molecular abundances (e.g., HCN, HNC), the huge abundance of cyanopolyynes, and the presence of polyynes and benzene (Cernicharo et al. 2001a, 2001b) and O-bearing molecules (Herpin & Cernicharo 2000). Ionic ([C II]) and atomic fine-structure lines ([O I]) are also detected as a result of the photodissociation of CO. At this stage, the main cooling of the gas occurs via CO high-J, [C II], and [O I] lines.

7. A YOUNG PN OBJECT: NGC 7027

NGC 7027 is the most evolved object in this study. It is a very young PN, having left the AGB only 10^3 yr ago (Volk & Kwok 1997). The estimated temperature of the central star is around 200,000 K (Latter et al. 2000). The gas in the inner 10″ radius of the envelope has been completely ionized, and a strong continuum emission arises from it. This region is revealed in the far-IR by fine-structure lines (Liu et al. 1996). The PDR at the interface between the ionized and neutral regions is mainly traced by the pure rotational lines of CH^+ (Cernicharo et al. 1997). The H_2 emission at this interface is found to be consistent with excitation by UV photons (Cox et al. 1997).

7.1. *Low-Excitation* CO *lines*

All the CO lines are asymmetrical (see Fig. 1), reflecting the complex kinematical structure of this PN. The main CO line emission is centered at $V_{LSR} \sim 27$–30 km s^{-1}, with an expansion velocity of 15 km s^{-1} for the $J = 1$–0, 2–1, 3–2, and 4–3 lines, and 20 km s^{-1} for the $J = 6$–5 and 7–6 lines (see Table 6). The higher velocity extent of the last two transitions probably indicates the presence of a faster wind at smaller radii (3″–5″). Jaminet et al. (1991) found $v_{exp} \sim 15$ km s^{-1} (with an angular extension of 5″–15″) for the $J = 2$–1 and 3–2 lines, in agreement with our data for those transitions. They also have derived a velocity dispersion as high as 3 km s^{-1} at small radii (less than 5″) and more than 1 km s^{-1} in the outer parts (greater than 5″). An absorption feature at $v_{LSR} \sim 10$ km s^{-1}, due to self-absorption (Jaminet et al. 1991), is detected in the low-J lines (see Fig. 1).

Although the $J = 1$–0 line of CO is certainly slightly contaminated by the 38α recombination line of atomic hydrogen (shifted only by -8.3 km s^{-1} with respect to its center),

TABLE 6

PARAMETERS FOR THE DIFFERENT FLOWS IN NGC 7027

CO LINE (J=)	v_{main} (km s^{-1})	v_{wing} (km s^{-1})	R_I	ΔR_I
1–0	14.6	47.2	0.04	(0.01)
2–1	14.3	43.2	0.09	(0.01)
3–2	16.0	30.0	0.07	(0.02)
4–3	18.3	25.1	0.07	(0.02)
6–5	20.0	24.7	0.06	(0.02)
7–6	20.0	23.8	0.09	(0.02)

NOTES.—The uncertainty on v_{main} and v_{wing} is 0.3 km s^{-1}. R_I is the wing and main integrated intensities ratio.

the line profiles also show some emission at high velocity (mainly in the red part) that could be the signature of a faster outflow, with an estimated velocity extent of 45 km s^{-1}. This outflow component was not reported by Jaminet et al. (1991). They only found the extended outflow with $v_{exp} \sim 15$ km s^{-1} and a wind at a smaller radius with $v_{exp} \sim 23$ km s^{-1}, which may be a flow driven by the pressure of the ionized region and which is probably the place where the $J = 6$–5 and 7–6 lines are mainly excited (see v_{main} in Table 6). The flow at higher velocity ($\sim$47 km s^{-1}) may be the relic of an HVW ejected during the PPN phase. Nevertheless, the importance of the wing emission is quite low, as the ratio R_I is less than 0.1.

7.2. *Far-IR Emission*

The $J = 14$–13 to $J = 23$–22 ^{12}CO lines are detected in the LWS grating spectrum of NGC 7027 and some ^{13}CO lines are also marginally detected. Despite its carbon-rich chemistry, several lines of OH are clearly identified (Liu et al. 1997), while no H_2O emission is observed (Cernicharo et al. 1997). In addition to the molecular emission, strong atomic and ionic features typical of a PN spectrum are also seen. They include [O I], [C II], [N II], [N III], and [O III] lines. The pure rotational lines of CH^+ discovered by Cernicharo et al. (1997) are prominent through the far-IR spectrum. Features at 149.18 and 180.7 μm correspond to rotational lines of CH (see Liu et al. 1997). A new feature of this species at 115.9 μm is tentatively detected. However, no HCN or HNC emission is seen, which supports the small HCN abundance (9×10^{-9}) derived by Deguchi et al. (1990). The main cooling agents are fine-structure atomic and ionic lines.

To fit the far-IR spectrum of NGC 7027 we have considered three components (see Table 7): (1) the atomic region, (2) a high-density layer, and (3) the AGB remnant. Sizes of the different regions are derived from Yan et al. (1999) and Jaminet et al. (1991).

The atomic region (region 1) has been subdivided into two layers, of 1000 K and $\theta = 5''$ and 800 K and $\theta = 6''$, respectively (Cernicharo et al. 1997; Liu et al. 1996; Hasegawa, Volk, & Kwok 2000). The density is 5×10^7 cm^{-3} and the expansion velocity 15 km s^{-1}. In the hottest layer, only [O I] and CH^+ are present (for now we have not considered [C II] and [O III] in the model, although they are also present). In the external layer, we introduce ^{12}CO, ^{13}CO, and OH. The considerable abundance of OH suggests that H_2O was probably present in the previous stage of evolution (see CRL 618) and, even if not detected, may be still present here, but with a low abundance. Thus, we placed H_2O in region 1, with an upper limit of abundance relative to H_2 of 1.5×10^{-7}, according to the present data. This upper limit is 50% lower than the one obtained by Volk & Kwok (1997). The best fit to the data gives the following abundances (relative to ^{12}CO) in this layer: less than 1/40, 1/20, 1/80, and 875 for ^{13}CO, OH, CH^+, and [O I], respectively. Comparing with analyses performed by other authors, we point out that the H_2 densities used in our model are higher than those of Liu et al. (1996), who took values between 10^5 and 10^6 cm^{-3} for the high-J CO lines coming from the hot region (1000–700 K). Also, the velocity of the expanding ionized region derived by Jaminet et al. (1991) is 17.6 km s^{-1}, while the estimated CO wind velocity by Sopka et al. (1989) is 17 km s^{-1}. Note that the two components of the atomic region produce similar lines, except that the hottest one only contains [O I] and CH^+.

In the high-density layer (region 2), we consider a temperature of 270 K, $\theta = 9''$, an expansion velocity of 15 km s^{-1}, and a density of 10^6 cm^{-3} (Yan et al. 1999; Justtanont et al. 2000). Volk & Kwok (1997) applied to this layer very similar values ($n_{H_2} = 9 \times 10^5$ cm^{-3} and $T = 220$ K). The fit results in a ^{12}CO column density of 2.1×10^{17} cm^{-2} and $^{12}CO/^{13}CO \leq 30$.

The AGB remnant (region 3) has an extension from $10''$ to $20''$; its gas temperature decreases from 100 to 50 K and its density from 3×10^5 to 10^4 cm^{-3} (Hasegawa et al. 2000). The expansion velocity is 15 km s^{-1} (see § 6.1 and Volk & Kwok 1997; Jaminet et al. 1991). The colder layer (50 K) is important here only to explain the low-J CO emission. The ^{12}CO column density is $(1.5$–$1.7) \times 10^{17}$ cm^{-2}, and the $^{12}CO/^{13}CO$ ratio is always less than 30. Note that CO emission extends over a region larger than $40''$ (Masson et al. 1985).

Our lower limit of the $^{12}C/^{13}C$ ratio (30) is compatible with the value derived by Kahane et al. (1992) for this object (65), using much more sensitive millimeter observations of several carbon-bearing molecules. The whole CO column density derived by Thronson (1983) is larger than 2×10^{17} cm^{-2}, in good agreement with our values.

The results of our model, when applied to the low-excitation CO lines, are satisfactory for $J = 1$–0 to $J = 4$–3, but the predicted intensities are too high for the $J = 6$–5 and 7–6 lines. The reason might be the complex kinematical structure of this PN.

7.3. *Changes Since the Previous Stage*

The main characteristic of this young PN, compared with previous stages, is the near disappearance of fast molecular winds. The hot central object induces a strong UV field, leading to a UV-dominated photochemistry in the envelope.

TABLE 7

Column Densities Obtained from Our Model for All Molecules Present in Each Region of NGC 7027

	Conditions				Column Density					
Region	T (K)	θ[a] (arcsec)	v (km s^{-1})	$n(H_2)$ (cm^{-3})	^{12}CO (cm^{-2})	^{13}CO (cm^{-2})	o-H_2O (cm^{-2})	OH (cm^{-2})	[O I] (cm^{-2})	CH^+ (cm^{-2})
Atomic region	1000	5	15	5×10^7	...	...	...	...	2×10^{19}	9×10^{13}
	800	6	15	5×10^7	8×10^{15}	2.7×10^{14}	$<2.6 \times 10^{13}$	4×10^{14}	7×10^{18}	10^{14}
High-density layer.....	270	9	10	10^6	2.1×10^{17}	7×10^{15}	...	...	...	...
Wind region	100	10	15	3×10^5	1.5×10^{17}	5×10^{15}	...	...	...	...
	50	20	15	10^4	1.7×10^{17}	5.7×10^{15}	...	...	...	...

[a] The solid angle of each considered layer.

As a consequence, molecular abundances have been strongly modified since the PPN phase. Water vapor and HCN have almost disappeared, while other species, such as CH^+, have been efficiently formed. The cooling effect of CO lines is much weaker, and now the gas is mainly cooling via ionic and atomic fine-structure lines.

8. DISCUSSION

It is assumed that CRL 2688 has just left the AGB phase: the central object is not yet sufficiently hot to produce a significant ionization or photodissociation of the gas. Hence, the far-IR molecular emission (^{12}CO, ^{13}CO, and HCN) is well reproduced by our model. Nevertheless, the detection of the polyynes C_4H_2 and C_6H_2 in this object indicates that some chemical processing has already started, an important difference with respect to IRC +10216, where these species are not detected.

In addition to the slowly expanding AGB CSE remnant, this PPN exhibits an inner and faster outflow, which runs into that AGB envelope. This is one of the main characteristics of an object beginning its transition to the PN stage. At this point, emission from the molecular gas is the main cooling process.

The ^{13}CO emission is not detectable at the low sensitivity of the LWS grating spectrum. For a ^{12}CO abundance of 6×10^{-4}, the upper limit of ^{13}CO abundance would be less than 2.2×10^{-5}. This value is half of what was found by Yamamura et al. 1996 (4×10^{-5} to 7.5×10^{-5}), but is similar to the ^{13}CO abundance found in an AGB star such as IRC +10216 [$(1–3) \times 10^{-5}$; Cernicharo et al. 1996]. However, Kahane et al. (1992) derived more accurate isotopic ratios, 3.7×10^{-5} and 7.5×10^{-5}, respectively, for IRC +10216 and CRL 2688, showing an increase by a factor of 2. For Jaminet et al. (1992), CNO nuclear processing in the star injects material into the stellar wind: in the slow wind $^{12}CO/^{13}CO = 20$, while in the fast wind they find a ratio of 5. Because of these values, these authors placed CRL 2688 among the *J*-type carbon stars, which have a considerably lower $^{12}CO/^{13}CO$ ratio than carbon stars (40–80). However, we prefer to argue that CRL 2688 has just begun to evolve to the PN stage; the ^{12}CO material has just begun to be reprocessed, as proved by the apparent increase of the ^{13}CO abundance between IRC +10216 and CRL 2688.

The HCN/CO ratio in IRC +10216 is 0.1, much larger than in the HVWs of the post-AGB envelopes discussed here. According to our model, we find a lower HCN abundance (relative to ^{12}CO) in the fast wind ($\leq 6 \times 10^{-6}$) than in the slow wind ($\leq 2 \times 10^{-5}$, i.e., similar to IRC+10216). Sopka et al. (1989) found 3.3×10^{-6} in the fast wind, while Jaminet et al. (1992) found 7×10^{-7}.

HNC is not detected in this object. This molecule is mainly formed by ion-molecule reactions, and in this post-AGB envelope, physical conditions are therefore not very suitable for considerable HNC production. Moreover, Yamamura et al. (1996) and Sopka et al. (1989) derived HCN/HNC $\sim$ 21 and 160, respectively. According to this, the HNC emission is largely under our detection limit.

In CRL 618, Herpin & Cernicharo (2000) have shown that O-bearing species, H_2O and OH, are produced in the innermost region of the CSE. Also Cernicharo et al. (2001a, 2001b) have detected in this object the polyacetylenic chains C_4H_2 and C_6H_2, methylpolyynes, and benzene. The UV photons from the central star photodissociate most of the molecular species produced in the AGB phase and allow a chemistry dominated by standard ion-neutral reactions. O-bearing species are formed, and also abundances of carbon-rich molecules, such as HCN and HNC, are modified (see Table 8). At the high temperatures of the PDR, OH can be formed by endothermic reactions between O and H_2, with O released by CO photodissociation, and then can produce H_2O through reactions with H_2. H_2O and OH can also be produced from the dissociative recombination of H_3O^+, if this ion is abundant enough.

TABLE 8

MOLECULAR, ATOMIC, AND IONIC ABUNDANCES (RELATIVE TO ^{12}CO), AS SEEN BY THE MODEL

Species	CRL 2688	CRL 618	NGC 7027
^{13}CO	<1/25	1/20	$\lesssim$1/30
HCN.....	<1/30–1/100	1/10–1/1000	...
HNC.....	...	1/10–1/1000	...
H_2O	...	1/25	<1/650
OH.....	...	1/1250	1/20
[O I].....	...	4.5	875
CH^+.....	...	...	1/80

NGC 7027 has a very hot central star. Because of the high UV flux ($10^4 \leq G_0 \leq 10^5$; Burton, Hollenbach, & Tielens 1990), there is a strong presence of atomic lines. UV photons from the central star produce a PDR, and the gas cools mainly via fine-structure atomic lines. In the PDR, the total number of CO molecules is around 2% of that of ionized carbon, i.e., most of the CO molecules have been photodissociated (Liu et al. 1996). As the ionized region is not modeled in this work, our results concerning the atomic region have to be carefully taken: in the high electron density environment of NGC 7027, ionic fine-structure lines are strongly suppressed by collisional de-excitation (Liu et al. 1996; Keyes, Aller, & Feibelman 1990). Electron impact may be important in exciting the CH^+ lines and would lower the CH^+ abundance (Cernicharo et al. 1997). In the 1000 K layer, the formation of CH^+ may be achieved via $C^+ + H_2 \rightarrow CH^+ + H$ (activation energy of $\sim$4000 K). The formation rate of CH^+ (Sternberg & Dalgarno 1995) could be high enough to produce column densities similar to those derived in this work. Because of the high temperatures, densities, and UV radiation field in the PDR, the formation of CH^+ leads to the creation of CH_2^+ and CH_3^+, whose dissociative recombination will form CH very efficiently at a temperature of 800 K (Sternberg & Dalgarno 1995); Liu et al. (1997) derived $CH/CH^+ \sim 0.2$. The observed CH lines are excited by collisions with atomic and molecular hydrogen.

The presence of [O I] and CH^+ in the 1000 K layer of the atomic region and the low abundance of CO in the 800 K layer indicate that the CO molecules have been largely reprocessed there through UV photons. Note that the chemical model of Hasegawa et al. (2000) shows that the CO observed in these objects consists of new formed molecules. Nevertheless, the AGB circumstellar gas has not been totally reprocessed: the ionized region and PDR still constitute a relatively small, but significant, fraction of the total mass of the circumstellar material around NGC 7027.

The study of CRL 618 showed that H_2O and OH can be efficiently produced. However, these O-bearing species are also quickly reprocessed. This is seen in the next stage, represented by NGC 7027. The equilibrium models (McCabe,

Connon Smith, & Clegg 1979) predict essentially no water in the carbon-rich conditions of the NGC 7027 envelope. Volk & Kwok (1997) argue that even under nonequilibrium chemical conditions, only a very small fraction of oxygen will be converted to water here. The nondetection of H_2O and the detection of OH in NGC 7027 indicate that H_2O molecules formed in the previous stage may have been almost entirely reprocessed. In the NGC 7027 environment, the simplest explanation for the water vapor disappearance is its transformation into OH and H by UV photodissociation. This will explain the increase of OH abundance by a factor of 60 since the previous, PPN stage, represented by CRL 618. Concerning HCN, probably most molecules have been photodissociated into H and CN (CN was detected by Bachiller et al. 1997 with a strong abundance, CN/HCN = 9). Photodissociation of CO, HCN, and other carbon-bearing molecules contribute to the increase of carbon ions abundance.

9. CONCLUSION

The study of the three selected objects in rapid evolution from the AGB to the PN stage clearly shows the crucial importance that (1) the interaction between fast and slow winds and (2) the increase of UV flux as the central object evolves toward the white dwarf state have on the chemistry. The spectroscopic evidence of the increasing UV flux comes from the appearance of atomic and ionic lines in CRL 618, which later dominate the far-IR spectrum of NGC 7027. Atomic and ionic lines tend to appear (at *ISO*'s sensitivity) when the central star is hotter than 10,000 K (Fong et al. 2001; Castro-Carrizo et al. 2001). On the other hand, the spectroscopic signature showing that shocks become less important as the evolution goes on comes from the wind velocity decrease seen in the CO profiles (this must be confirmed by further studies on more objects and only refers to the neutral gas). The strongest shocks occur just after the star leaves the AGB, when the central star is ejecting large amounts of material in a very fast wind (the case of CRL 2688). The AGB remnant envelope is being shocked by an inner, faster wind developed in the PPN stage (i.e., the 200 km s^{-1} wind in CRL 618). Most of the ^{12}CO, ^{13}CO, and HCN emission is produced in these shocks. The rapid increase of the stellar temperature will produce a new, UV-dominated chemistry when $T_{\rm eff} \geq 30,000$ K. These new conditions (UV photons and shocks) will deeply modify the constitution of the inner parts of the envelope. Indeed, in CRL 618, O-bearing molecules (H_2O and OH; Herpin & Cernicharo 2000) and relatively complex organic molecules (Cernicharo et al. 2001a, 2001b) appear. Furthermore, most of the CO and HCN will be entirely reprocessed in the PDR, leading to strong HNC emission. At this point, CO and [O I] atomic lines are the dominant coolants.

As the star reaches the PN stage, the strong, fast molecular winds have disappeared, and slow expanding layers constitute the PN envelope around a large and hot atomic region. Most of the *old* AGB material has been reprocessed. The spectrum is now dominated by atomic and ionic lines. New species, such as CH^+ and CH, appear. There is only weak HCN emission, as the molecules may have been broken into H and CN. More interesting is the disappearance of H_2O, which has probably also been reprocessed and is only a relatively abundant molecule in the intermediate, carbon-rich PPN stage.

We thank Spanish DGES, CICYT, and PNIE for funding support for this research under grants PB96-0883, ESP98-1351E, and PANAYA2000-1784. J. R. G. acknowledges UAM for a predoctoral fellowship. J. R. P. also acknowledges further support for his research from NSF grants AST 99-80846 (CSO operations) and ATM 96-16766. We thank V. Bujarrabal for useful comments and suggestions. We thank the anonymous referee for his useful comments, which resulted in an important improvement of this paper.

REFERENCES

Acker, A., Ochsenbein, F., Stenholm, B., Tylenda, R., Marcout, J., & Schohn, C. 1992, Strasbourg-ESO Catalogue of Galactic Planetary Nebulae (Garching: ESO)
Bachiller, R., Forveille, T., Huggins, P. J., & Cox, P. 1997, A&A, 324, 1123
Bernard Salas, J., Pottasch, S. R., Beintema, D. A., & Wesselius, P. R. 2001, A&A, 367, 949
Bujarrabal, V., & Alcolea, J. 1991, A&A, 251, 536
Bujarrabal, V., Castro-Carrizo, A., Alcolea, J., & Sánchez Contreras, C. 2001, A&A, 377, 868
Bujarrabal, V., Fuente, A., & Omont, A. 1994, A&A, 285, 247
Bujarrabal, V., Gómez-González, J., Bachiller, R., & Martín-Pintado, J. 1988, A&A, 204, 242
Burton, M. G., Hollenbach, D. J., & Tielens, A. G. G. M. 1990, ApJ, 365, 620
Carsenty, U., & Solf, J. 1982, A&A, 106, 307
Castro-Carrizo, A., Bujarrabal, V., Fong, D., Meixner, M., Tielens, A. G. G. M., Latter, W. B., & Barlow, M. J. 2001, A&A, 367, 674
Cernicharo, J., Guélin, M., & Kahane, C. 2000, A&AS, 142, 181
Cernicharo, J., Guélin, M., Martín-Pintado, J., Peñalver, J., & Mauersberger, R. 1989, A&A, 222, L1
Cernicharo, J., Heras, A. M., Pardo, J. R., Tielens, A. G. G. M., Guélin, M., Dartois, E., Neri, R., & Waters, L. B. F. M. 2001a, ApJ, 546, L127
Cernicharo, J., Heras, A. M., Tielens, A. G. G. M., Pardo, J. R., Herpin, F., Guélin, M., & Waters, L. B. F. M. 2001b, ApJ, 546, L123
Cernicharo, J., Liu, X.-W., González-Alfonso, E., Cox, P., Barlow, M. J., Lim, T., & Swinyard, B. M. 1997, ApJ, 483, L65
Cernicharo, J., Yamamura, I., González-Alfonso, E., de Jong, T., Heras, A., Escribano, R., & Ortigoso, J. 1999, ApJ, 526, L41
Cernicharo, J., et al. 1996, A&A, 315, L201
Cox, P., Lucas, R., Huggins, P. J., Forveille, T., Bachiller, R., Guilloteau, S., Maillard, J. P., & Omont, A. 2000, A&A, 353, L25
Cox, P., et al. 1996, A&A, 315, L265
———. 1997, A&A, 321, 907
Crosas, M., & Menten, K. M. 1997, ApJ, 483, 913
Deguchi, S., Izumiura, H., Kaifu, N., Mao, X., Nguyen-Q-Rieu, & Ukita, N. 1990, ApJ, 351, 522
Fong, D., Meixner, M., Castro-Carrizo, A., Bujarrabal, V., Latter, W. B., Tielens, A. G. G. M., Kelly, D. M., & Sutton, E. C. 2001, A&A, 367, 652
Frank, A., Balick, B., Icke, V., & Mellema, G. 1993, ApJ, 404, L25
Fuente, A., Cernicharo, J., & Omont, A. 1998, A&A, 330, 232
Glassgold, A. E. 1996, ARA&A, 34, 241
Groenewegen, M. A. T. 1997, A&A, 317, 503
Groenewegen, M. A. T., van der Veen, W. E. C. J., & Matthews, H. E. 1998, A&A, 338, 491
Hajian, A. R., Phillips, J. A., & Terzian, Y. 1996, ApJ, 467, 341
Hasegawa, T., Volk, K., & Kwok, S. 2000, ApJ, 532, 994
Herpin, F., & Cernicharo, J. 2000, ApJ, 530, L129
Hora, J. L., Deutsch, L. K., Hoffmann, W. F., & Fazio, G. G. 1996, AJ, 112, 2064
Jaminet, P. A., Danchi, W. C., Sandell, G., & Sutton, E. C. 1992, ApJ, 400, 535
Jaminet, P. A., Danchi, W. C., Sutton, E. C., Russell, A. P. G., Sandell, G., Bieging, J. H., & Wilner, D. 1991, ApJ, 380, 461
Jura, M., & Kroto, H. 1990, ApJ, 351, 222
Justtanont, K., Tielens, A. G. G. M., Skinner, C. J., & Haas, M. R. 1997, ApJ, 476, 319
Justtanont, K., et al. 2000, A&A, 360, 1117
Kahane, C., Cernicharo, J., Gómez-González, J., & Guélin, M. 1992, A&A, 256, 235
Kahane, C., Dufour, E., Busso, M., Gallino, R., Lugaro, M., Forestini, M., & Straniero, O. 2000, A&A, 357, 669
Keyes, C. D., Aller, L. H., & Feibelman, W. A. 1990, PASP, 102, 59
Kooi, J. W., et al. 2000, Int. J. Infrared Millimeter Waves, 21, 1357
Kwok, S. 2000, in The Origin and Evolution of Planetary Nebulae (Cambridge: Cambridge Univ. Press)
Kwok, S., Su, K. Y. L., & Stoesz, J. A. 2001, in Post-AGB Objects as a Phase of Stellar Evolution, ed. R. Szczerba & S. K. Górny (Dordrecht: Kluwer), 115

Latter, W. B., Dayal, A., Bieging, J. H., Meakin, C., Hora, J. L., Kelly, D. M., & Tielens, A. G. G. M. 2000, ApJ, 539, 783
Liu, X.-W., et al. 1996, A&A, 315, L257
———. 1997, MNRAS, 290, L71
———. 2001, MNRAS, 323, 343
Loup, C., Forveille, T., Omont, A., & Paul, J. F. 1993, A&AS, 99, 291
Lucas, R., & Guélin, M. 1999, in IAU Symp. 191, Asymptotic Giant Branch Stars, ed. T. Le Bertre, A. Lèbre, & C. Waelkens (San Francisco: ASP), 305
Martín-Pintado, J., Gaume, R. A., Johnston, K. J., & Bachiller, R. 1995, ApJ, 446, 687
Masson, C. R., et al. 1985, ApJ, 292, 464
Mauron, N., & Huggins, P. J. 1999, A&A, 349, 203
McCabe, E. M., Connon Smith, R., & Clegg, R. E. S. 1979, Nature, 281, 263
Men'shchikov, A. B., Balega, Y., Blöcker, T., Osterbart, R., & Weigelt, G. 2001, A&A, 368, 497
Meixner, M., Fong, D., Sutton, E. C., & Welch, W. J. 2001, in Post-AGB Objects as a Phase of Stellar Evolution, ed. R. Szczerba & S. K. Górny (Dordrecht: Kluwer), 369
Neri, R., García-Burillo, S., Guélin, M., Cernicharo, J., Guilloteau, S., & Lucas, R. 1992, A&A, 262, 544
Neufeld, D. A., & Melnick, G. J. 1990, ApJ, 352, L9
Neufeld, D. A., & Melnick, G. J. 1991, ApJ, 368, 215 (erratum, 374, 784)
Omont, A., et al. 1995, ApJ, 454, 819
Penzias, A. A., & Burrus, C. A. 1973, ARA&A, 11, 51
Sahai, R., et al. 1998, ApJ, 493, 301
Skinner, C. J., Meixner, M., & Bobrowsky, M. 1998, MNRAS, 300, L29
Sopka, R. J., Olofsson, H., Johansson, L. E. B., Nguyen-Q-Rieu, & Zuckerman, B. 1989, A&A, 210, 78
Speck, A. K., Meixner, M., & Knapp, G. R. 2000, ApJ, 545, L145
Sternberg, A., & Dalgarno, A. 1995, ApJS, 99, 565
Thronson, H. A., Jr. 1983, ApJ, 264, 599
Tsuji, T. 1973, A&A, 23, 411
Volk, K., & Kwok, S. 1997, ApJ, 477, 722
Volk, K., Xiong, G.-Z., & Kwok, S. 2000, ApJ, 530, 408
Yamamura, I., Onaka, T., Kamijo, F., Deguchi, S., & Ukita, N. 1996, ApJ, 465, 926
Yamamura, I., Shibata, K. M., Kasuga, T., & Deguchi, S. 1994, ApJ, 427, 406
Yan, M., Federman, S. R., Dalgarno, A., & Bjorkman, J. E. 1999, ApJ, 515, 640
Young, K., Serabyn, G., Phillips, T. G., Knapp, G. R., Güsten, R., & Schulz, A. 1992, ApJ, 385, 265
Zuckerman, B., & Aller, L. H. 1986, ApJ, 301, 772